Original Article

3D morphometry using automated aortic segmentation in native MR angiography: an alternative to contrast enhanced MRA?

Matthias Müller-Eschner[1,2], Tobias Müller[1], Andreas Biesdorf[3], Stefan Wörz[3], Fabian Rengier[1,2], Dittmar Böckler[4], Hans-Ulrich Kauczor[1], Karl Rohr[3], Hendrik von Tengg-Kobligk[1,2,5]

[1]Department of Diagnostic and Interventional Radiology, University Hospital Heidelberg, Germany; [2]Department of Radiology, German Cancer Research Center, Heidelberg, Germany; [3]Dept. Bioinformatics and Functional Genomics, Biomedical Computer Vision Group, University of Heidelberg, BIOQUANT, IPMB, and DKFZ Heidelberg; [4]Department of Vascular and Endovascular Surgery, University Hospital Heidelberg, Germany; [5]Institute of Diagnostic, Interventional and Pediatric Radiology, University Hospital Bern, Inselspital, Bern, Switzerland

Correspondence to: Hendrik von Tengg-Kobligk, M.D. Institute of Diagnostic, Interventional and Pediatric Radiology (DIPR), University Hospital of Bern, Inselspital, CH-3010 Bern, Switzerland. Email: Hendrik.vonTengg@insel.ch.

Introduction: Native-MR angiography (N-MRA) is considered an imaging alternative to contrast enhanced MR angiography (CE-MRA) for patients with renal insufficiency. Lower intraluminal contrast in N-MRA often leads to failure of the segmentation process in commercial algorithms. This study introduces an in-house 3D model-based segmentation approach used to compare both sequences by automatic 3D lumen segmentation, allowing for evaluation of differences of aortic lumen diameters as well as differences in length comparing both acquisition techniques at every possible location.

Methods and materials: Sixteen healthy volunteers underwent 1.5-T-MR Angiography (MRA). For each volunteer, two different MR sequences were performed, CE-MRA: gradient echo Turbo FLASH sequence and N-MRA: respiratory-and-cardiac-gated, T2-weighted 3D SSFP. Datasets were segmented using a 3D model-based ellipse-fitting approach with a single seed point placed manually above the celiac trunk. The segmented volumes were manually cropped from left subclavian artery to celiac trunk to avoid error due to side branches. Diameters, volumes and centerline length were computed for intraindividual comparison. For statistical analysis the Wilcoxon-Signed-Ranked-Test was used.

Results: Average centerline length obtained based on N-MRA was 239.0±23.4 mm compared to 238.6±23.5 mm for CE-MRA without significant difference (P=0.877). Average maximum diameter obtained based on N-MRA was 25.7±3.3 mm compared to 24.1±3.2 mm for CE-MRA (P<0.001). In agreement with the difference in diameters, volumes obtained based on N-MRA (100.1±35.4 cm^3) were consistently and significantly larger compared to CE-MRA (89.2±30.0 cm^3) (P<0.001).

Conclusions: 3D morphometry shows highly similar centerline lengths for N-MRA and CE-MRA, but systematically higher diameters and volumes for N-MRA.

Keywords: Magnetic resonance angiography; aorta; thoracic; automatic data processing

Submitted Sep 12, 2013. Accepted for publication Oct 28, 2013.
doi: 10.3978/j.issn.2223-3652.2013.10.06
View this article at: http://www.thecdt.org/article/view/2980/4516

Introduction

High-resolution imaging of the aorta is essential for preoperative planning and follow-up of patients with aortic disease (1). Today multidetector computed tomography (MDCT) is the gold standard to assess aortic pathologies before and after treatment because it has the advantages of high spatial resolution, short acquisition time and wide availability. On the downside, patients with aortic disease are often repeatedly exposed to a significant amount of ionizing radiation and nephrotoxic contrast agents with the risk to induce renal insufficiency, especially in this compromised patient group with a high incidence of

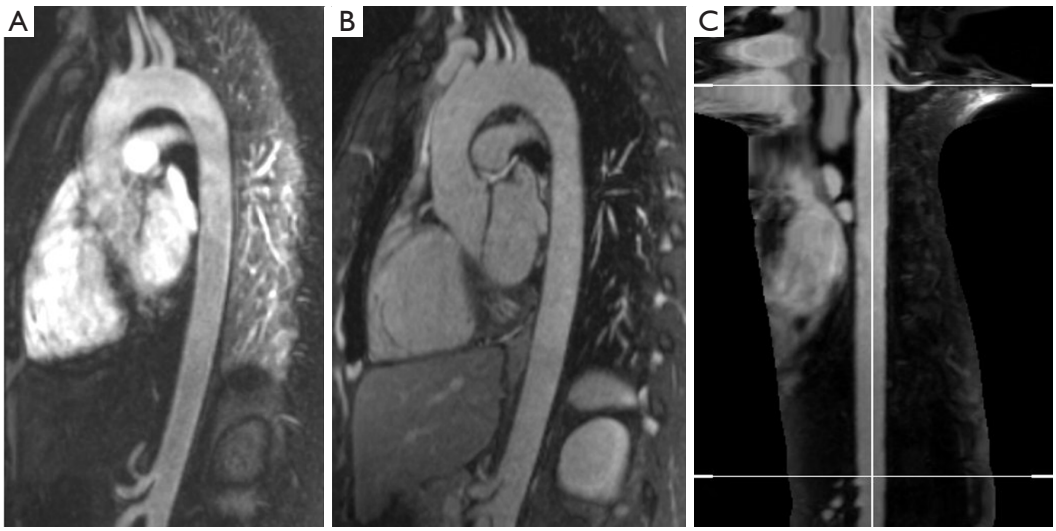

Figure 1 Contrast-enhanced (CE-MRA) (A) and native magnetic resonance angiography (N-MRA) (B) as well as centerline length measurement based on a CE-MRA dataset (C).

coexistent cardiovascular and renovascular disease.

Consequently magnetic resonance imaging (MRI) is considered an alternative to MDCT prior and after aortic treatment (2-6). Advances in MRI imaging allow for acquisition of high-resolution ECG- and respiratory-triggered MRA datasets by use of the steady-state-free precession technique (SSFP) [further referred to as native magnetic resonance angiography (N-MRA)] without the need for intravenous contrast administration (*Figure 1*) (7-11).

In the last year, several studies investigated the value of N-MRA for imaging and diameter assessment of the thoracic aorta with accurate results compared to contrast-enhanced magnetic resonance angiography (CE-MRA) or MDCT datasets (5,7,9-13). However, diameters were always assessed manually giving way for high inter- and intraobserver variability. Lowest inter- and intraobserver variability is achieved if diameter and length are measured based on centerline analysis with automatic lumen segmentation on dedicated post-processing workstations (14,15).

However, lower signal-to-noise-ratio and therefore lower intraluminal contrast in N-MRA datasets challenge the segmentation process of commercial algorithms. To overcome this problem and to exactly compare differences between N-MRA and CE-MRA exams we introduce an in-house 3D model-based segmentation approach (16). To our knowledge there is no study comparing both sequences by automatic 3D lumen segmentation, allowing for evaluation of differences in aortic lumen diameters as well as differences in length comparing both acquisition techniques at every possible location.

The purpose of this study was therefore to assess diameter, area, volume and length differences between N-MRA and CE-MRA using an in-house developed 3D model-based segmentation approach.

Material and methods

Study collective

Sixteen healthy volunteers (4 females, 12 males) with a mean age of 50±14 years (range, 31-69 years), a body weight of 77±12 kg (range, 62-110 kg), and a height of 172±9 cm (range, 160-191 cm) were included in this prospective, single-center study. The study was approved by the local institutional review board; oral and written informed consent was obtained from all volunteers prior to MRA examination.

MR imaging technique

Examinations were performed using a standard clinical 1.5 T whole-body scanner (Magnetom Avanto®, Siemens Medical Solutions, Erlangen, Germany). Two phased array body coils were placed on the thorax and abdomen (supine position). The scanner's integrated ECG gating unit was used. Two different MR sequences were compared, both acquired in a para-sagittal plane aligned with the curvature

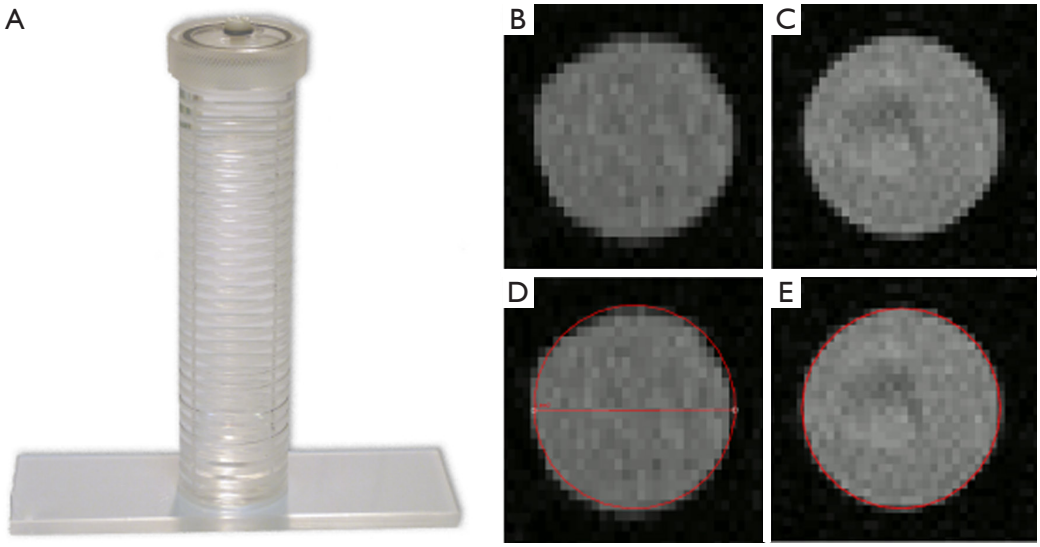

Figure 2 Tubular phantom (A) and automatic segmentation of contrast-enhanced (CE-MRA) (B,D) and native magnetic resonance angiography (N-MRA) (C,E) datasets.

of the aortic arch.

(I) CE-MRA (*Figure1A*): a T1-weighted gradient echo Turbo FLASH sequence was oriented sagittal-oblique and aligned along the aortic arch with the following parameters: TE =1.06 ms; TR =2.9 ms; flip angle 25°, bandwidth =650 Hz/Pixel, matrix =384×288, FoV was kept constant resulting in an inplane resolution =1.2 mm × 1.2 mm, slice thickness =1.6 mm; 60 slices per slab (slab thickness =96 mm), iPAT factor (GRAPPA) =2. Acquisition was performed in an expiratory breath-hold of 22±2 s. Contrast enhancement was achieved with 0.15 mmol/kg body weight of gadobenate dimeglumine (Gd- BOPTA, MultiHance®, Bracco Imaging, Konstanz, Germany) administered via an ante-cubital vein at 3 mL/s, followed by a saline chaser of 30 mL with the same injection rate. To determine the individual circulation time, a test bolus measurement was performed beforehand using 1 mL of contrast medium and a 2D axial T1-weighted GRE sequence at the level of the descending aorta.

(II) N-MRA (*Figure 1B*): a T2-prepared, ECG-triggered 3D steady-state free precession (N-MRA) sequence was oriented sagittal-oblique and aligned along the aortic arch with a navigator (NAV) at the level of the diaphragm: TE =1.57 ms, echo spacing =3.7 ms, TR =241 ms, flip angle 90°, bandwidth =530 Hz/Pixel, Matrix =256×168, FoV was kept constant, resulting in an inplane resolution = 1.2 mm × 1.2 mm, slice thickness =1.3 mm; 40 slices per slab (slab thickness =52 mm), iPAT factor (GRAPPA)=2. The navigator gating window was ±3.5 mm. The N-MRA was performed during "free-breathing" and required 14±5 mins for data acquisition. The trigger delay was individually adjusted to obtain data acquisition into the diastole. The navigator was not online adapting.

Phantom

To evaluate accuracy of the automatic model based segmentation approach and to appraise differences between both MRI sequences *ex vivo* excluding *in vivo* factors (e.g., aortic, heart, lung movement) a tubular phantom with known dimensions was scanned.

The phantom consists of a straight acrylic tube with an inner diameter of 31.5 mm and a length of 150 mm (*Figure 2A*).

Prior to acquisition of the CE-MRA sequence the phantom was filled with a mixture of 0.05 mL Gd-chelate (Gd-DOTA, Dotarem®, Guerbet, France) and 117 mL deionized water. For acquisition of the N-MRA sequence the phantom was filled with deionized water only.

Image analysis

For 3D segmentation of the phantom (*Figure 2B-E*) and volunteer datasets (*Figure 3*), we developed an automatic 3D model-based segmentation approach consisting of two steps. In the first step, we determine a coarse segmentation of the aorta using a cylindrical intensity model with circular

Figure 3 Model based segmentation of native magnetic resonance angiography datasets (N-MRA) (A,B).

cross-sections. The model is directly fitted to the 3D image data through an incremental process based on a Kalman filter (16). As a result, we obtain a dense set of 200-300 vessel segments representing the 3D geometry of the aorta. In the second step, we compute a refinement for each vessel segment using a different model with elliptical cross-sections to determine minimum and maximum diameters (17). An advantage of our model-based approach is that quantitative information such as the different diameters, cross-section area, and centerline length are directly accessible from the segmentation result.

The segmented volumes of volunteer datasets were manually cropped from left subclavian artery to celiac trunk to avoid error due to supra aortic and abdominal side branches. Mean (D_{mean}), minimum (D_{min}) and maximum diameter (D_{max}) as well as cross-sectional area (Area) in the resulting volume of interest were computed for individual comparison. Furthermore, centerline length (*Figure 1C*) and volume of the segmentation of the aortic lumen were calculated.

Statistical analysis

Wilcoxon-Signed-Ranked-Test (PASW for Windows, Version 17) was used to test for significant differences of measurements obtained from both sequences (N-MRA and CE-MRA). Furthermore a Bland-Altman analysis was performed to assess their respective level of agreement. A P value <0.05 was considered statistically significant.

Results

Accuracy of automatic segmentation approach in vitro

For the phantom data the 3D model-based segmentation approach yielded submillimeter accuracy with a mean segmentation error for D_{mean}, D_{min} and D_{max} between 0.1-0.6 mm regarding the true value of the tubular phantom (*Table 1*) for both the CE-MRA and N-MRA datasets. At the given in-plane resolution (1.2 mm × 1.2 mm) this error was below 0.5 voxels. Comparing the absolute measurements no differences larger than 1mm in diameter could be observed between CE-MRA and N-MRA sequences. There was also high agreement for area between both sequences (*Table 1*).

Differences between both sequences in vivo

Automatic 3D model-based segmentation of all volunteer datasets was successful and the resulting segmented volume of interest is shown in *Figure 3A*. Note the elliptic shape of the model-fit in *Figure 3B*. For the volunteer datasets average centerline length obtained based on N-MRA was 239.0±23.4 mm compared to 238.6±23.5 mm for CE-MRA showing no significant difference (P=0.877). Average mean diameter D_{mean} obtained based on N-MRA was 22.5±3.4 mm compared to 21.4±3.1 mm for CE-MRA (P<0.001). In all cases D_{max} obtained from the N-MRA measurements was significantly larger with a mean difference of 1.6 mm (95% limits of agreement from –0.1-3.2 mm) (*Figure 4A*). Resulting

Table 1 Avg and error of D_{min}, D_{max} and D_{mean} as well as area assessment in the phantom using the elliptical model based on CE-MRA and N-MRA datasets. True, known dimensions of the phantom are given under the column true

	True	CE-MRA		N-MRA	
		Avg	Error	Avg	Error
D_{min} (mm)	31.5	31.6±0.1	0.1±0.1	31.6±0.2	0.1±0.1
D_{max} (mm)	31.5	32.1±0.1	0.6±0.1	32.0±0.2	0.5±0.2
D_{mean} (mm)	31.5	31.8±0.1	0.3±0.1	31.8±0.1	0.3±0.1
Area (mm²)	779.3	795.1±3.1	15.8±3.1	793.8±2.8	14.5±2.8

Avg, Average; D_{min}, minimum diameter; D_{max}, maximum diameter; D_{mean}, mean diameter; CE-MRA, contrast-enhanced magnetic resonance angiography; N-MRA, native magnetic resonance angiography.

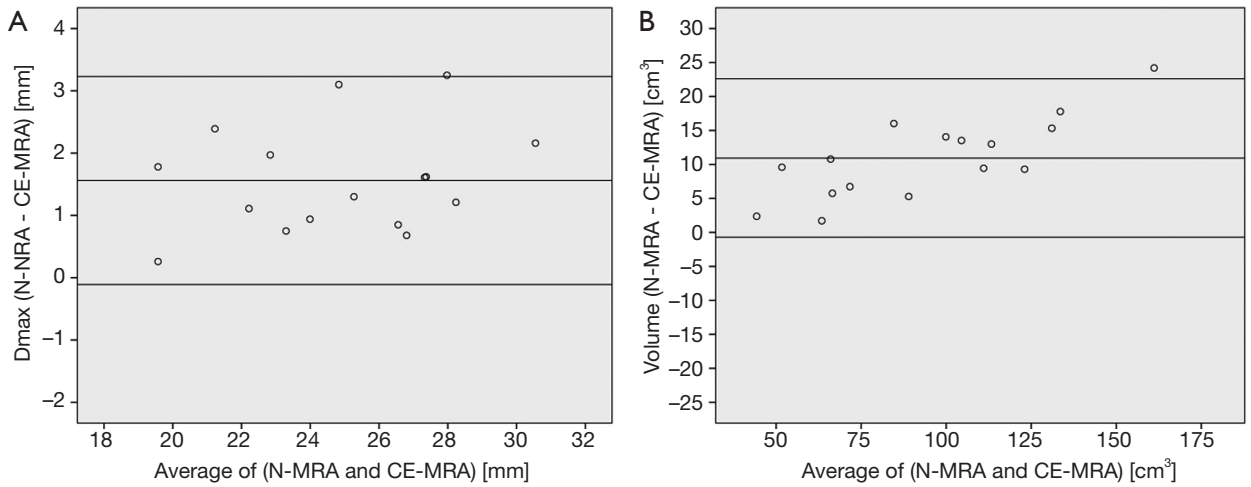

Figure 4 Bland Altman plot of differences in maximum diameter (D_{max}) (A) and calculated segmented volume (B) from native- (N-MRA) and contrast-enhanced (CE-MRA) magnetic resonance angiography datasets.

Table 2 Avg range and P value of automatic model-based measurements of volume, centerline length, D_{min}, D_{max}, D_{mean} and area obtained from CE-MRA and N-MRA datasets

	CE-MRA		N-MRA		P
	Avg	Range	Avg	Range	
Vol (cm³)	89.2±30.8	43.1-149.0	100.1±35.5	45.5-173.2	0.001
Centerline (mm)	238.6±23.5	205.6-280.0	239.0±23.4	205.8-278.0	0.877
D_{min} (mm)	18.9±2.6	14.3-22.8	20.0±2.9	15.0-24.3	0.001
D_{max} (mm)	24.1±3.2	18.7-29.5	25.7±3.3	19.7-31.6	0.001
D_{mean} (mm)	21.4±3.1	16.3-26.2	22.5±3.4	16.7-28.1	0.001
Area (mm²)	366.2±104.0	208.5-541.9	409.9±119.7	220.1-623.6	0.001

Avg, Average; centerline, centerline length; D_{min}, minimum diameter; D_{max}, maximum diameter; D_{mean}, mean diameter; CE-MRA, contrast-enhanced magnetic resonance angiography; N-MRA, native magnetic resonance angiography.

from larger values in diameter and cross-sectional area, volumes obtained based on N-MRA (100.1±35.4 cm³) were consistently and significantly larger compared to CE-MRA (89.2±30.0 cm³) (P<0.001) (*Table 2*, *Figure 4B*). Mean

Table 3 Bland Altman analysis and limits of agreement calculated as ±1.96 SD of differences in volume, centerline length, D_{min}, D_{max}, D_{mean} and area assessment between N-MRA and CE-MRA datasets

	N-MRA—CE-MRA	
	Avg	Limits of agreement*
Vol (cm^3)	10.9±5.9	–0.7-22.6
Centerline (mm)	0.4±2.4	–4.3-5.1
D_{min} (mm)	1.1±0.8	–0.5-2.6
D_{max} (mm)	1.6±0.9	–0.1-3.2
D_{mean} (mm)	1.2±0.5	0.2-2.3
Area (mm^2)	43.7±21.7	1.2-86.2

*Calculated as ±1.96 SD. Avg, Average; Centerline, centerline length; D_{min}, minimum diameter; D_{max}, maximum diameter; D_{mean}, mean diameter; CE-MRA, contrast-enhanced magnetic resonance angiography; N-MRA, native magnetic resonance angiography.

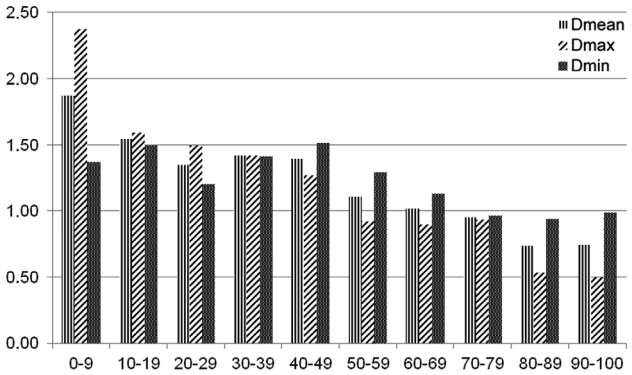

Figure 5 Differences in average diameter [minimum (D_{min}), maximum (D_{max}), mean (D_{mean})] between native- and contrast-enhanced magnetic resonance angiography datasets at different locations of the descending aorta (0-100%, 0%= left subclavian artery, 100%= proximal celiac trunk).

difference between two average diameter measurements for a pair of datasets was 1.2±0.5 mm (*Table 3*). However, difference in diameter measurements decreased continuously from the left subclavian artery to the celiac trunk (*Figure 5*).

Discussion

The 3D model-based segmentation approach yielded highly accurate results segmenting the lumen of the phantom; differences compared to true dimension were within submillimeter or subvoxel range, respectively. There was no significant difference for *in vitro* measurements between both sequences.

Aortic dimensions in healthy volunteers assessed by N-MRA were generally larger compared to CE-MRA datasets (mean difference: D_{min} 1.1 mm, D_{mean} 1.1 mm, D_{max} 1.6 mm), most difference sensitively reflected by differences in aortic area (mean 43.7 mm^2). Morphometric differences were largest distal to the left subclavian artery (mean difference: D_{mean} 1.9 mm) with decreasing differences towards the celiac trunk (mean difference: D_{mean} 0.7 mm). However, considering the MR sequences' through-plane spatial resolution of 1.3-1.6 mm, differences between both sequences were only in subvoxel or voxel range.

Our data is in accordance with a recently published study that also reports larger intraluminal diameters in N-MRA (ECG-triggered 3D-navigated free breathing bSSFP), compared to CE-MRA datasets in diameter measurements of the ascending aorta (11).

In vivo, various factors could explain the differences observed in both sequences. Whereas in our study the CE-MRA sequence was acquired during breath-hold, the N-MRA was acquired during free breathing. A recently published study evaluated differences in aortic diameter between N-MRA (ECG-triggered 2D breath-hold SSFP sequence with SENSE) and CE-MRA datasets with both sequences acquired during breath-hold. The authors report a mean difference of 1 mm in the descending aorta (9) and lower values for the N-MRA. Changes of intra-thoracic pressure during breath-hold or free breathing might therefore influence assessment of aortic diameter in both sequences.

An earlier study of our group assessing aortic displacement in healthy volunteers revealed that displacement decreases from the aortic arch to the celiac trunk (18). Due to the fact that differences observed between the two sequences are highest at the aortic arch with almost continuous decrease to the celiac trunk suggests that aortic displacement might also be an important factor influencing differences between both sequences.

Compared to the gold standard multidetector computed tomography (MDCT) variation of vessel diameter in the thoracic aorta and supra aortic branches in pigs compared to N-MRA (ECG-triggered, 3D-navigated free breathing bSSFP) was 0.5 mm. Unfortunately, CE-MRA was not part of this protocol (7).

Further studies with a higher number of subjects are needed to assess which of both sequences best reflects true

intraluminal dimension *in vivo*.

Due to the fact that extrinsic contrast agent is not necessary; indications for N-MRA are various. Examination time is not limited by contrast passing, therefore acquisition of high resolution ECG—and respiratory triggered datasets is possible and especially useful in evaluation of the thoracic and especially ascending aorta where correct diameter assessment is limited in CE-datasets due to motion artifacts.

Furthermore it is useful in patients with impaired renal function that are prone to renal insufficiency when given nephrotoxic contrast agent in MDCT, or nephrogenic systemic fibrosis when given gadolinium chelate based contrast agent in MRI (19). We acknowledge the following limitations of our study. Even though in-plane resolution was the same for both sequences, slice thickness of the CE-MRA was 0.3 mm larger than for the N-MRA Furthermore, the CE-MRA acquisition was not ECG gated. However, ECG-gating would have required to under sample the k-space with subsequent loss of spatial resolution to avoid an increase in acquisition time. In the context of translation into clinical routine the authors are aware that healthy volunteers were investigated and no patients. This is the reason why we could not compare MRA to CTA datasets. For methodological purposes we aimed to further investigate our new model-based segmentation approach under best conditions and avoid possible artifacts.

In this early stage of evaluating the 3D model-based segmentation approach for CE- and N-MRA and comparing both sequences, side branches were disregarded to exclude potential errors due to motion artifacts as well as segmentation challenges.

In conclusion 3D morphometric assessment is possible with the presented 3D segmentation approach and the results show highly similar centerline lengths for N-MRA and CE-MRA. However, there is a systematic increase in intraluminal diameter and volume for N-MRA compared to CE-MRA especially in the proximal descending aorta. Further studies are warranted to assess which of both sequences represents true aortic dimensions the best.

Acknowledgements

Matthias Müller-Eschner and Hendrik von Tengg-Kobligk received support from the German Research Foundation (DFG) within project R03, SFB/TRR 125 "Cognition-Guided Surgery". Karl Rohr and Stefan Wörz acknowledge the support of the German Research Foundation (DFG) within the project QuantVessel (RO 2471/6). Andreas Biesdorf has been supported by the International Graduate School of the German Cancer Research Center (DKFZ).
Disclosure: The authors declare no conflict of interest.

References

1. von Tengg-Kobligk H, Weber TF, Ley S, et al. State-of-the-art aortic imaging [Aktuelle Bildgebung der Aorta]. Gefässchirurgie 2009;14:143-57.
2. Ludman CN, Yusuf SW, Whitaker SC, et al. Feasibility of using dynamic contrast-enhanced magnetic resonance angiography as the sole imaging modality prior to endovascular repair of abdominal aortic aneurysms. Eur J Vasc Endovasc Surg 2000;19:524-30.
3. Neschis DG, Fairman RM. Magnetic resonance imaging for planning aortic endograft procedures. Semin Vasc Surg 2004;17:135-43.
4. Neschis DG, Velazquez OC, Baum RA, et al. The role of magnetic resonance angiography for endoprosthetic design. J Vasc Surg 2001;33:488-94.
5. Gebker R, Gomaa O, Schnackenburg B, et al. Comparison of different MRI techniques for the assessment of thoracic aortic pathology: 3D contrast enhanced Mr angiography, turbo spin echo and balanced steady state free precession. Int J Cardiovasc Imaging 2007;23:747-56.
6. Resta EC, Secchi F, Giardino A, et al. Non-contrast Mr imaging for detecting endoleak after abdominal endovascular aortic repair. Int J Cardiovasc Imaging 2013;29:229-35.
7. Ley-Zaporozhan J, Kreitner KF, Unterhinninghofen R, et al. Assessment of thoracic aortic dimensions in an experimental setting: comparison of different unenhanced magnetic resonance angiography techniques with electrocardiogram-gated computed tomography angiography for possible application in the pediatric population. Invest Radiol 2008;43:179-86.
8. Krishnam MS, Tomasian A, Malik S, et al. Image quality and diagnostic accuracy of unenhanced SSFP Mr angiography compared with conventional contrast-enhanced Mr angiography for the assessment of thoracic aortic diseases. Eur Radiol 2010;20:1311-20.
9. Groth M, Henes FO, Müllerleile K, et al. Accuracy of thoracic aortic measurements assessed by contrast enhanced and unenhanced magnetic resonance imaging. Eur J Radiol 2012;81:762-6.
10. Krishnam MS, Tomasian A, Deshpande V, et al.

Noncontrast 3D steady-state free-precession magnetic resonance angiography of the whole chest using nonselective radiofrequency excitation over a large field of view: comparison with single-phase 3D contrast-enhanced magnetic resonance angiography. Invest Radiol 2008;43:411-20.
11. Potthast S, Mitsumori L, Stanescu LA, et al. Measuring aortic diameter with different Mr techniques: comparison of three-dimensional (3D) navigated steady-state free-precession (SSFP), 3D contrast-enhanced magnetic resonance angiography (CE-MRA), 2D T2 black blood, and 2D cine SSFP. J Magn Reson Imaging 2010;31:177-84.
12. Srichai MB, Kim S, Axel L, et al. Non-gadolinium-enhanced 3-dimensional magnetic resonance angiography for the evaluation of thoracic aortic disease: a preliminary experience. Tex Heart Inst J 2010;37:58-65.
13. von Tengg-Kobligk H, Ley-Zaporozhan J, Henninger V, et al. Intraindividual assessment of the thoracic aorta using contrast and non-contrast-enhanced Mr angiography. Rofo 2009;181:230-6.
14. Müller-Eschner M, Rengier F, Partovi S, et al. Accuracy and variability of semiautomatic centerline analysis versus manual aortic measurement techniques for TEVAR. Eur J Vasc Endovasc Surg 2013;45:241-7.
15. Rengier F, Weber TF, Partovi S, et al. Reliability of semiautomatic centerline analysis versus manual aortic measurement techniques for TEVAR among non-experts. Eur J Vasc Endovasc Surg 2011;42:324-31.
16. Wörz S, von Tengg-Kobligk H, Henninger V, et al. 3-D quantification of the aortic arch morphology in 3-D CTA data for endovascular aortic repair. IEEE Trans Biomed Eng 2010;57:2359-68.
17. Biesdorf A, Wörz S, Müller T, et al. Model-based segmentation and motion analysis of the thoracic aorta from 4D ECG-gated CTA images. Med Image Comput Comput Assist Interv 2011;14:589-96.
18. Rengier F, Weber TF, Henninger V, et al. Heartbeat-related distension and displacement of the thoracic aorta in healthy volunteers. Eur J Radiol 2012;81:158-64.
19. Broome DR. Nephrogenic systemic fibrosis associated with gadolinium based contrast agents: a summary of the medical literature reporting. Eur J Radiol 2008;66:230-4.

Cite this article as: Müller-Eschner M, Müller T, Biesdorf A, Wörz S, Rengier F, Böckler D, Kauczor HU, Rohr K, von Tengg-Kobligk H. 3D morphometry using automated aortic segmentation in native MR angiography: an alternative to contrast enhanced MRA? Cardiovasc Diagn Ther 2014;4(2):80-87. doi: 10.3978/j.issn.2223-3652.2013.10.06

